THE MOTION AND SPIN EVOLUTION OF EXTENDED BODIES IN ROTATING BLACK HOLE SPACETIMES

ZOLTÁN KERESZTES[1], BALÁZS MIKÓCZI[2]

[1]*Department of Theoretical Physics, University of Szeged, Tisza Lajos krt 84-86, 6720 Szeged, Hungary*
Email: zkeresztes@titan.physx.u-szeged.hu
[2]*Research Institute for Particle and Nuclear Physics, Wigner RCP, H-1525 Budapest 114, P.O. Box 49, Hungary*

Abstract. We investigate the evolution of spinning bodies moving along unbound orbits in different rotating (singular/regular) black hole spacetimes. The evolutions describe such scattering processes during which the bodies enter the ergosphere of the rotating black holes but remain outside of the outer event horizon. The considered orbits run close to the equatorial plane. We illustrate the spin influences on the orbit dynamics and that the spin precessional angular velocity is highly increased near and within the ergosphere. The scattering processes are characterized by the final values of spin and orbital plane orientation angles and azimuthal Boyer-Lindquist coordinate. Their dependencies on the initial spin angles and a characteristic black hole parameter are discussed.

Key words: General Relativity – Gravitation – Black hole – Celestial Mechanics.

1. INTRODUCTION

In the general relativity in both presence and absence of standard model matter fields any black hole solution contains a spacetime singularity where the validity of the theory breaks. However in the presence of non-standard matter fields, singularity free spacetime solutions describing black holes can be obtained. In the recent years, these regular black holes have been widely studied, see for example Refs. Bianchi *et al.* (2015); Toshmatov *et al.* (2015); Abdujabbarov *et al.* (2016); Maluf and Neves (2018); Toshmatov *et al.* (2019).

The first metric characterizing a spacetime of a non-rotating regular black hole was proposed by Bardeen (Bardeen, 1968). This metric was interpreted as describing the spacetime surrounding a magnetic monopole which occurs in a nonlinear electrodynamics (Ayón-Beato and García, 2000). The nonlinear electrodynamics is constructed in terms of an antisymmetric electromagnetic field tensor as the Maxwell theory but the Lagrangian is modified. A nonrotating regular black hole spacetime was also proposed by Hayward (Hayward, 2006) having similar interpretation with another Lagrangian for the nonlinear electrodynamics (Fan and Wang, 2016). A more generic metric containing the subcases suggested by Bardeen and Hayward, and in-

cluding the rotation of the black hole was derived in Ref. Toshmatov *et al.* (2017a), which we will consider in this paper.

In order to discover the distinguishability of singular and regular black hole spacetimes we consider the evolution of extended * spinning bodies moving along unbound orbits. Note that hyperbolic orbits of spinning bodies about singular black holes in the extreme mass ratio limit were already investigated by using the Matthison-Papapetrou-Dixon (MPD) equations (Bini *et al.*, 2017a). Analytic computations in Ref. Bini *et al.* (2017a) were carried out for small spin magnitudes whose direction is parallel to the central black hole rotation axis and when the body moves in the equatorial plane. In this configuration the spin direction is conserved. In our investigation the spin axis is not parallel to the black hole rotation axis. As a consequence, the orbit of the body is not confined precisely to the equatorial plane and the spin direction evolves. In addition the closest approach distance during the evolution is inside the ergosphere where a post-Newtonian approximation fails. Therefore we use the MPD equations for description of the evolution.

The paper is organized as follow. In Section 2 we introduce the MPD equations, the metric characterizing the spacetime of the considered rotating, singular/regular black holes, and two fundamental families of observers, the static and the zero angular momentum ones. We set two frames of co-moving observers by boosting the static and the zero angular momentum observers' frames and describe the spin evolution in them. In Section 3 the discussion of scattering processes based on numerical simulations are presented while Section 4 contains the conclusions.

2. THE DYNAMICS OF THE EXTENDED BODIES IN ROTATING, REGULAR BLACK HOLE SPACETIMES

2.1. EVOLUTION EQUATIONS

The MPD equations (Mathisson, 1937; Papapetrou, 1951; Dixon, 1970, 1976) describe the motion of an extended spinning body in curved spacetime in the pole-dipole approximation, which read as

$$\frac{\mathrm{D}p^a}{\mathrm{d}\tau} = -\frac{1}{2}R^a{}_{bcd}u^b S^{cd}\,, \tag{1}$$

$$\frac{\mathrm{D}S^{ab}}{\mathrm{d}\tau} = p^a u^b - u^a p^b\,. \tag{2}$$

*An extended body is described by an infinite series of multipole moments (Dixon, 1964). A point-like particle only has the monopole moment. The body in the Matthison-Papapetrou-Dixon model (used in this paper) is described in the pole-dipole approximation when it is characterized by mass and spin, with all the higher multipoles neglected.

Here $\mathrm{D}/\mathrm{d}\tau = u^c\nabla_c$ is the covariant derivative along the integral curve of the four velocity u^a obeying the normalization $u^a u_a = -1$, $R^a_{\ bcd}$ is the Riemann tensor of the background spacetime, and p^a and S^{ab} are the four-momentum and the spin tensor of the moving body, respectively. The MPD equations are closed with a spin supplementary condition (SSC) which determines the representative point for the extended body. In this paper we use the Tulczyjew-Dixon (TD) SSC (Tulczyjew, 1959; Dixon, 1970) imposing $p_a S^{ab} = 0$. This SSC together with the MPD equations results in two constants of motion: the spin magnitude $S = \sqrt{S_{cd}S^{cd}/2}$ and the dynamical mass $M = \sqrt{-p^a p_a}$. The TD SSC and the MPD equations yield the following velocity-momentum relation (Semerák, 1999):

$$u^b = \frac{m}{M^2}\left(p^b + \frac{2S^{ba}R_{aecd}p^e S^{cd}}{4M^2 + R_{aecd}S^{ae}S^{cd}}\right) , \tag{3}$$

where $m = -u_a p^a$ is the mass measured in the rest frame of the observer moving with velocity u^a.

In addition, we introduce a spin four vector as

$$S^a = -\frac{1}{2M}\eta^{abcd}p_b S_{cd} , \tag{4}$$

where η_{abcd} is the 4-dimensional Levi-Civita tensor which is totally antisymmetric and $\eta_{0123} = \sqrt{-g}$, where g is the determinant of the metric.

2.2. ROTATING, REGULAR BLACK HOLES

The considered line element squared in Boyer-Lindquist coordinates (t, r, θ, ϕ) (Toshmatov *et al.*, 2017a)[†] is given by

$$\begin{aligned} \mathrm{d}s^2 &= -\frac{\Delta - a^2\sin^2\theta}{\Sigma}\mathrm{d}t^2 - \frac{2a\mathcal{B}\sin^2\theta}{\Sigma}\mathrm{d}t\mathrm{d}\phi \\ &\quad + \frac{\Sigma}{\Delta}\mathrm{d}r^2 + \Sigma\mathrm{d}\theta^2 + \frac{\mathcal{A}}{\Sigma}\sin^2\theta\mathrm{d}\phi^2 , \end{aligned} \tag{5}$$

where a is the rotation parameter,

$$\Sigma = r^2 + a^2\cos^2\theta , \tag{6}$$

$$\Delta = r^2 + a^2 - 2\alpha(r)\, r , \tag{7}$$

$$\mathcal{B} = r^2 + a^2 - \Delta , \tag{8}$$

[†]There are discussions (Bronnikov, 2017; Rodrigues and Junior, 2017; Toshmatov *et al.*, 2017b) on that the rotating regular black hole spacetime presented in Ref. Toshmatov *et al.* (2017a) is not an exact solution of the field equations. However it is proved that the presented spacetime may differ only perturbatively from the exact solution (Toshmatov *et al.*, 2017b), therefore it is suitable for consideration of spinning bodies evolutions.

and

$$\mathcal{A} = \left(r^2 + a^2\right)^2 - \Delta a^2 \sin^2\theta \, . \tag{9}$$

The function $\alpha(r)$ is

$$\alpha(r) = \mu + \frac{\mu_{em} r^\gamma}{(r^\nu + q_m^\nu)^{\gamma/\nu}} \, . \tag{10}$$

For a vacuum spacetime $\mu_{em} = 0$, and μ represents the mass parameter of the black hole. In this case (5) reduces to the Kerr metric (Kerr, 1963). When a nonlinear electrodynamic field is present in the spacetime, $\mu_{em} = q_m^3/\sigma \neq 0$ is interpreted as an electromagnetically induced ADM mass (Toshmatov *et al.*, 2018). The quantity σ in the expression of μ_{em} controls the strength of the nonlinear electrodynamic field and carries the dimension of length squared while q_m is related to the magnetic charge (Fan and Wang, 2016). The spacetime is free from the singularity for $\mu = 0$ and $\gamma \geq 3$. In the case of $\mu = 0$ and $\mu_{em} \neq 0$, the powers (γ,ν) are (3,2) for the Bardeen and (3,3) for the Hayward subcases (Toshmatov *et al.*, 2017a).

The stationary limit surfaces and the event horizons (if they exist) are determined by the solutions of $g_{tt} = 0$ and $g^{rr} = 0$, respectively. The region which is located outside the outer event horizon but inside the outer stationary limit surface is called ergosphere. The existence of the stationary limit surfaces and the event horizons are strongly dependent on the parameter q_m, see Figs. 3 and 4 in Ref. Toshmatov *et al.* (2017a). For the chosen parameter values in the next section, the regular black holes will have similar structure like the Kerr spacetime, *i.e.* they have two event horizons and two stationary limit surfaces and the spacetime contains an ergosphere in all cases.

In the following we introduce two family of observers. The frame of the static observers (SOs) is given by the tetrad

$$\begin{aligned} e_{\mathbf{0}} &= \frac{1}{\sqrt{-g_{tt}}}\partial_r \, , \, e_{\mathbf{1}} = \sqrt{\frac{\Delta}{\Sigma}}\partial_r \, , \, e_{\mathbf{2}} = \frac{\partial_\theta}{\sqrt{\Sigma}} \, , \\ e_{\mathbf{3}} &= -\frac{1}{\sqrt{\Delta}}\left(\frac{a\mathcal{B}\sin\theta}{\Sigma\sqrt{-g_{tt}}}\partial_t - \frac{\sqrt{-g_{tt}}}{\sin\theta}\partial_\phi\right) \, , \end{aligned} \tag{11}$$

while that of the zero angular momentum observers (ZAMOs) by

$$\begin{aligned} f_{\mathbf{0}} &= \sqrt{\frac{\mathcal{A}}{\Sigma\Delta}}\left(\partial_t + \frac{a\mathcal{B}}{\mathcal{A}}\partial_\phi\right) \, , \, f_{\mathbf{1}} = \sqrt{\frac{\Delta}{\Sigma}}\partial_r \, , \\ f_{\mathbf{2}} &= \frac{\partial_\theta}{\sqrt{\Sigma}} \, , \, f_{\mathbf{3}} = \sqrt{\frac{\Sigma}{\mathcal{A}}}\frac{\partial_\phi}{\sin\theta} \, . \end{aligned} \tag{12}$$

Following Ref. Bini *et al.* (2017b), we define Cartesian-like 3-bases $(e_{\mathbf{x}}, e_{\mathbf{y}}, e_{\mathbf{z}})$ and $(f_{\mathbf{x}}, f_{\mathbf{y}}, f_{\mathbf{z}})$ in the local rest spaces of the SOs and the ZAMOs by $(e_{\mathbf{1}}, e_{\mathbf{2}}, e_{\mathbf{3}})$

$= (e_{\mathbf{x}}, e_{\mathbf{y}}, e_{\mathbf{z}})\, R(\theta, \phi)$ and $(f_{\mathbf{1}}, f_{\mathbf{2}}, f_{\mathbf{3}}) = (f_{\mathbf{x}}, f_{\mathbf{y}}, f_{\mathbf{z}})\, R(\theta, \phi)$, respectively, where

$$R(\theta, \phi) = \begin{pmatrix} \sin\theta\cos\phi & \cos\theta\cos\phi & -\sin\phi \\ \sin\theta\sin\phi & \cos\theta\sin\phi & \cos\phi \\ \cos\theta & -\sin\theta & 0 \end{pmatrix} \tag{13}$$

is the same rotation matrix which locally relates the unit basis vectors of Cartesian and spherical coordinates in the 3-dimensional Euclidean space. The orbit of the spinning body will be represented in the coordinate space

$$\begin{aligned} x &= r\cos\phi\sin\theta\ , \\ y &= r\sin\phi\sin\theta\ , \\ z &= r\cos\theta\ . \end{aligned} \tag{14}$$

We characterize the instantaneous plane of the motion in the (x, y, z)-space by the unit vector:

$$\mathbf{l} = \frac{\mathbf{R}\times\mathbf{V}}{|\mathbf{R}\times\mathbf{V}|}\ , \tag{15}$$

where $\times$ is the cross product in Euclidean 3-space, $\mathbf{R}$ is the position vector with components:

$$R^{\mathbf{x}} = x\ ,\ R^{\mathbf{y}} = y\ ,\ R^{\mathbf{z}} = z\ , \tag{16}$$

and $\mathbf{V}$ is a spatial velocity vector with [‡]

$$V^{\mathbf{x}} = \frac{\mathrm{d}x}{\mathrm{d}\tau}\ ,\ V^{\mathbf{y}} = \frac{\mathrm{d}y}{\mathrm{d}\tau}\ ,\ V^{\mathbf{z}} = \frac{\mathrm{d}z}{\mathrm{d}\tau}. \tag{17}$$

The absolute value in the denominator denotes the "Euclidean length" of the numerator. Since the considered spacetimes are asymptotically flat, the quantity $l^{\mathbf{i}}$ coincides with the direction of the orbital angular momentum[§] at the spatial infinity.

We describe the spin dynamics in the comoving frame obtained by boost transformations from the frames of the static and zero angular momentum observers. When boosting the static observer's frame we obtain the co-moving frame as

$$E_{\mathbf{0}}(u) = u\ ,\ E_{\alpha}(e, u) = e_{\alpha} + \frac{u\cdot e_{\alpha}}{1+\Gamma_{(S)}}\left(u + u_{(SO)}\right)\ , \tag{18}$$

[‡]Noting that we could use any timelike parameter in the definition (17) due to the normalisation in Eq. (15).

[§]We mention that the natural definition of orbital angular momentum about x_0 would be

$$L^{ab} = -\sigma^{[a}(x, x_0)\, p^{b]}(\tau)\ .$$

Here σ^a is a generalized position vector which can be computed from the Synge's world function (Synge, 1960). However there are only few metrics for which the exact world function is known (Ruse, 1930; Gunther, 1965; Buchdahl, 1972; Buchdahl and Warner, 1980; John, 1984, 1989; Roberts, 1993).

with $u_{(SO)} = e_{\mathbf{0}}$, $\Gamma_{(S)} = -u \cdot u_{(SO)}$ and $\alpha = \{\mathbf{1}, \mathbf{2}, \mathbf{3}\}$, while boosting the zero angular momentum observer's frame we have

$$E_{\mathbf{0}}\left(u\right) = u \ , \ E_{\alpha}\left(f, u\right) = f_{\alpha} + \frac{u \cdot f_{\alpha}}{1 + \Gamma_{(Z)}} \left(u + u_{(ZAMO)}\right) \ , \tag{19}$$

with $u_{(ZAMO)} = f_{\mathbf{0}}$ and $\Gamma_{(Z)} = -u \cdot u_{(ZAMO)}$. Here the dot denotes the inner product with respect to the background spacetime metric. A spatial rotation about the axis n^{α} with non-vanishing components

$$n^{\mathbf{1}} = -\frac{w^{\mathbf{2}}_{(Z)}}{\sqrt{\left(w^{\mathbf{1}}_{(Z)}\right)^2 + \left(w^{\mathbf{2}}_{(Z)}\right)^2}} \text{ and } n^{\mathbf{2}} = \frac{w^{\mathbf{1}}_{(S)}}{\sqrt{\left(w^{\mathbf{1}}_{(S)}\right)^2 + \left(w^{\mathbf{2}}_{(S)}\right)^2}} \tag{20}$$

by an angle Θ determined from

$$\sin\Theta = -\left[\left(1 - \sqrt{\frac{\Sigma\Delta}{-g_{tt}\mathcal{A}}}\right)\frac{\Gamma_{(S)} w^{\mathbf{3}}_{(S)}}{1 + \Gamma_{(S)}} - \frac{a\mathcal{B}\sin\theta}{\sqrt{-g_{tt}\Sigma\mathcal{A}}}\right] \frac{\Gamma_{(S)}\sqrt{\left(w^{\mathbf{1}}_{(S)}\right)^2 + \left(w^{\mathbf{2}}_{(S)}\right)^2}}{1 + \Gamma_{(Z)}} \ , \tag{21}$$

transforms the frame vectors $E_{\mathbf{A}}\left(e, u\right)$ to $E_{\mathbf{A}}\left(f, u\right)$ (where $\mathbf{A} = \{\mathbf{0}, \mathbf{1}, \mathbf{2}, \mathbf{3}\}$). Here $\mathbf{w}_{(S)} = \Gamma^{-1}_{(S)} u_{(SO)} - u$ and $\mathbf{w}_{(Z)} = \Gamma^{-1}_{(Z)} u_{(ZAMO)} - u$ are the relative spatial velocities of the SO and ZAMO, respectively, with respect to the moving body in the co-moving frame.

When boosting the Cartesian-like SO and ZAMO frames we obtain the respective co-moving Cartesian-like frames which are also spatially rotated with respect to each other. The spin evolution in the co-moving Cartesian frame is described by the precession angle velocity:

$$\Omega^{\beta}_{(prec)} = -\Omega^{\beta}_{(orb)} + \Omega^{\beta} \ , \tag{22}$$

where $\Omega^{\beta}_{(orb)}$ is given by Eq. (87) of Ref. (Bini *et al.*, 2017b), and $\Omega^{\mathbf{1}} = E_{\mathbf{3}} \cdot \mathrm{D}E_{\mathbf{2}}/\mathrm{d}\tau$, $\Omega^{\mathbf{2}} = -E_{\mathbf{3}} \cdot \mathrm{D}E_{\mathbf{1}}/\mathrm{d}\tau$ and $\Omega^{\mathbf{3}} = E_{\mathbf{2}} \cdot \mathrm{D}E_{\mathbf{1}}/\mathrm{d}\tau$ (Bini *et al.*, 2017b). The $\Omega^{\beta}_{(prec)}(e, u)$ and $\Omega^{\beta}_{(prec)}(f, u)$ denote precession angle velocities in the boosted SO and ZAMO co-moving Cartesian frames, respectively.

3. NUMERICAL INVESTIGATION

We consider the evolution of spinning bodies following unbound orbits. During the evolution the bodies cross through the ergosphere of the rotating black holes at the closest approach. Regarding the rotating black hole we investigate three cases: $i)$ Kerr black hole ($\mu \neq 0$ and $\mu_{em} = 0$); $ii)$ rotating Hayward regular black hole ($\mu = 0$, $\mu_{em} \neq 0$, $\gamma = 3$ and $\nu = 3$); and rotating Bardeen regular black hole ($\mu = 0$, $\mu_{em} \neq 0$,

$\gamma = 3$ and $\nu = 2$). The rotation parameter is chosen as $a = 0.99\tilde{\mu}$ with $\tilde{\mu} = \mu$ for Kerr spacetime and $\tilde{\mu} = \mu_{em}$ for regular black holes.

For the numerical investigation the initial position of the body is chosen as

$$\theta(0) = \pi/2, r(0) = 2000\tilde{\mu}\ ,\ \phi(0) = 0 = t(0)\ , \tag{23}$$

and the independent components of the initial four momentum as

$$p^r(0)/M = -0.9, \tilde{\mu}p^{\phi}(0)/M = 8 \times 10^{-7}\ ,\ \tilde{\mu}p^{\theta}(0)/M = 0\ . \tag{24}$$

With these initial values we guarantee that the body will remain in the equatorial plane if it has no spin or its spin axis is aligned or anti-aligned with the rotation axis of the central black hole. In addition the initial spin vector of the body is characterized in the comoving Cartesian frame set up by boosting the SO frame. Then

$$S = S^{\mathbf{i}} E_{\mathbf{i}}(e, u)\ , \tag{25}$$

where $\mathbf{i} = \{\mathbf{x}, \mathbf{y}, \mathbf{z}\}$ and

$$S^{\mathbf{i}} = |S| \left(\cos\phi^{(S)} \sin\theta^{(S)}, \sin\phi^{(S)} \sin\theta^{(S)}, \cos\theta^{(S)}\right)\ . \tag{26}$$

The angles $\theta^{(S)}$ and $\phi^{(S)}$ are the spherical polar angles of the spin vector in the comoving Cartesian frame. The validity of the MPD dynamics requires the spin magnitude $|S|/\tilde{\mu}M$ to be small which is chosen as $|S|/\tilde{\mu}M = 0.01$ (Hartl, 2003).

We note that in case of Kerr spacetime, with a corresponding rescaling of coordinates and introducing dimensionless variables the parameters μ and M can be eliminated from the numeric consideration. Similarly, following Ref. Toshmatov *et al.* (2017a) for regular black holes, it can be achieved that only the combination

$$q = \frac{q_m}{\mu_{em}}\ , \tag{27}$$

enters explicitly in the numeric equations given in terms of dimensionless variables. The spacetime is only regular for $q \neq 0$ while the limit $q \to 0$ results in the Kerr spacetime with mass parameter $\mu = \mu_{em}$ (Toshmatov *et al.*, 2017a). For the regular Bardeen ($\nu = 2$) and Hayward ($\nu = 3$) subcases there is a black hole in the spacetime for $q \leq 0.081$ and $q \leq 0.216$, respectively. The event horizon disappears for higher values of q.

On Fig. 1 the evolutions of spinning bodies in different spacetimes are shown. The initial spin angles are chosen as $\phi^{(S)}(0) = \pi/2$ and $\theta^{(S)}(0) = \pi/2$. The three columns represent the following parameter choices for the background spacetime: rotating Hayward black hole with $q = 0.081$ (left column) and with $q = 0.216$ (middle column) and rotating Bardeen black hole with $q = 0.081$ (right column). The evolution in a Kerr spacetime with mass parameter $\mu = \mu_{em}$ is barely distinguishable from the case presented in the left column, therefore it is not shown separately. The first row depicts the unbound orbits in the (x,y,z)-space. The initial and the final

positions of the body are marked by green and red dots, respectively. The second and third rows represent the same orbit in the near region of the black hole in the (x,y,z) and the $(\rho = r\sin\theta, z = r\cos\theta)$ coordinate spaces. In the second row the red and the blue surfaces at the centre depict the inner (the outer event horizon) and outer (the outer stationary limit surface) bounds of the black hole's ergosphere, respectively. In the third row the inner and outer bounds of the ergosphere are indicated by red and blue curves. As the body enters in the ergosphere it makes two turns about the black hole, then it leaves the ergosphere going to the spatial infinity. The fourth and fifth rows image the spin vector represented in the boosted SO and ZAMO Cartesian frames, respectively. Since SOs only exist outside of the ergosphere, the spin evolution cannot be represented in the boosted SO frame when the body stays in that region. The jump in the evolution of the spin vector in the boosted SO frame (marked by black dots) emphasizes that a relatively large part of the variation in the spin direction takes place inside the ergosphere.

On Fig. 2, we show the evolutions of the rotation angle Θ defined by Eq. (21) (first row) and the spherical co-moving triad components of the precessional angular velocities $\Omega^{\alpha}_{(prec)}(e,u)$ and $\Omega^{\alpha}_{(prec)}(f,u)$ when the body is close to the central black hole. The purplish shadow represent that period where the body is inside the ergosphere. The angle Θ is small when the body is relatively far from the central black hole. Where this angle is small both boosted frames (SO and ZAMO) can be equally used for description of the spin dynamics. The blue lines representing the precessional velocity triad components in the boosted SO frame diverge at the location of the outer stationary surface. This is because SOs only exist outside of the ergosphere, thus the boosted SO frame cannot be used for description of the spin evolution at that location. However the boosted ZAMO frame can be used and the red curves show that the spin precessional velocities are highly increased within the ergosphere.

The increased spin precession near the ergosphere can be supported without using a particular frame. Fig. 3 shows the Boyer-Lindquist coordinate components of the unit spin vector S^a/S and their derivatives in case of a central rotating Hayward regular black hole with $q = 0.216$. The first and the second rows show the evolution of the Boyer-Lindquist coordinate components of the unit spin vector and their derivatives on the total considered timescale, respectively. While the third row represents these evolutions in that period where the body is close to the central black hole. The panels show that the unit spin vector coordinate components and their derivatives undergo significant changes when the body is near and inside the ergosphere.

In the forthcoming we investigate the variation of the final spin and orbital plane orientation (given by Eq. (15)) angles as functions of initial spin angles and the black hole parameter q. The polar and azimuthal angles of the instantaneous orbital plane orientation will be denoted by $\theta^{(l)}$ and $\phi^{(l)}$, respectively. For $\tau > \tau^* = 4500\tilde{\mu}$, the angles $\theta^{(l)}$, $\phi^{(l)}$, $\theta^{(S)}$ and $\phi^{(S)}$ undergo only unsignificant changes, thus we

characterize the scattering process with their values at τ^*.

The polar angles $\theta^{(s)}(\tau^*)$ and $\theta^{(l)}(\tau^*)$ are shown on Fig. 3 in the parameter space of initial spin angles $\theta^{(s)}(0)$ and $\phi^{(s)}(0)$. These color maps are independent from the chosen background spacetime (Kerr, Hayward or Bardeen). The left panel expresses that $\theta^{(s)}(\tau)$ is almost a constant. The right panel shows that $\theta^{(l)}(\tau)$ also undergoes only a small variation which is the largest for the initial spin angles $\theta^{(s)}(0) \approx 3\pi/7...4\pi/7$.

On Figs. 5 and 3 we present the azimuthal angles $\phi^{(s)}(\tau^*)$ and $\phi^{(l)}(\tau^*)$ in the parameter space of $\left[\theta^{(s)}(0), \phi^{(s)}(0)\right]$, respectively. From top left to bottom right the background spacetimes are Kerr, rotating Hayward with $q = 0.081$, rotating Hayward with $q = 0.216$ and rotating Bardeen with $q = 0.081$. The red lines on both sides represent the cases when the azimuthal angles $\phi^{(s)}$ and $\phi^{(l)}$ are indefinite because then the spin is parallel/anti-parallel with the rotation axis of the central black hole during the whole evolution and the body remains in the equatorial plane. For another initial values the spin is precessing and we show the cumulative value of $\phi^{(s)}$. However for the azimuthal angle of the orbital orientation we present $\tilde{\phi}^{(l)}(\tau^*) = \phi^{(l)}(\tau^*) \mod 2\pi$. This is because $\theta^{(l)}(\tau)$ vanishes multiple times and then $\phi^{(l)}$ becomes undetermined. On both figures the panels in the first lines share more similarities. The local maxima of $\phi^{(s)}$ are in the following $\left[\theta^{(s)}(0), \phi^{(s)}(0)\right]$ domains $[5\pi/7..6\pi/7, 10\pi/7..12\pi/7]$ and $[9\pi/10..\pi, 5\pi/7..6\pi/7]$ on all panels. These local maxima are decreasing from top left to bottom right. The maximum of $\phi^{(l)}$ is in the domain $[5\pi/7..6\pi/7, 12\pi/7..2\pi]$ for the first two panel while in $[2\pi/7..3\pi/7, 0..2\pi/7]$ for the third one and $[5\pi/7..6\pi/7, 0..2\pi/7]$ for the fourth panel.

In the considered cases the orbit of the spinning body is confined close to the equatorial panel. Therefore the value of the Boyer-Lindquist coordinate ϕ at τ^* is also good parameter for the characterization of the scattering process. Its value in the parameter space of $\left[\theta^{(s)}(0), \phi^{(s)}(0)\right]$ is presented on Fig. 7. The picture shows that $\phi(\tau^*)$ is independent from $\phi^{(s)}(0)$ while it is an increasing function of $\theta^{(s)}(0)$.

The Figs. 5, 3 and 7 proves that the values $\phi^{(s)}(\tau^*)$, $\tilde{\phi}^{(l)}(\tau^*)$ and $\phi(\tau^*)$ depend on the parameters of the background spacetime and the most significant changes occurs in $\phi(\tau^*)$.

On Fig. 3 and 9 we present the dependence of the final values of spin angles and orbital plane orientation angles, respectively, on the parameters q and $\phi^{(s)}(0)$ in rotating Hayward (left column) and Bardeen (right column) spacetimes, remembering that $q \to 0$ corresponds to the Kerr limit. For these figures the initial polar spin angle is chosen as $\theta^{(s)}(0) \approx \pi/2$. Interestingly the color maps on the left and right hand sides are similar to each other but it must be emphasized that the ranges of q are very different. Apart from some relatively small domains, we find higher values for the considered angles at fixed q in case of rotating Hayward background.

Table 1

The coefficients α, h, δ and ω of the shifted sine function at different q values in case of a central rotating Hayward black hole, see Fig. 11

q	α	h	δ	ω
0	-0.1109	4.5542	1.5361	0.9998
0.031	-0.1108	4.5533	1.5361	0.9998
0.062	-0.1101	4.5467	1.5364	0.9998
0.093	-0.1081	4.5292	1.5371	0.9998
0.123	-0.1044	4.4960	1.5384	0.9998
0.154	-0.0988	4.4440	1.5403	0.9999
0.185	-0.0915	4.3720	1.5429	1.0000
0.216	-0.0829	4.2810	1.5460	1.0001

Table 2

The coefficients α, h, δ and ω of the shifted sine function at different q values in case of a central rotating Bardeen black hole, see Fig. 11

q	α	h	δ	ω
0	-0.1109	4.5542	1.5361	0.9998
0.012	-0.1100	4.5451	1.5364	0.9998
0.023	-0.1071	4.5182	1.5373	0.9998
0.035	-0.1027	4.4752	1.5388	0.9998
0.046	-0.0970	4.4181	1.5406	0.9999
0.058	-0.0907	4.3498	1.5427	1.0000
0.069	-0.0839	4.2729	1.5450	1.0000
0.081	-0.0771	4.1900	1.5473	1.0001

Since $\phi(\tau^*)$ does not depend on $\phi^{(s)}(0)$ we depict it on Fig. 10 as a function of q and $\theta^{(s)}(0)$ with a fixed value of $\phi^{(s)}(0) = 0$. It turns out that the dependence of $\phi(\tau^*)$ on $\theta^{(s)}(0)$ at fixed q can be described by a simple shifted sine function which is shown on Fig. 11 for rotating Hayward (top panel) and Bardeen (bottom panel) black holes. The values denoted by the dots are determined numerically and the function $\alpha \sin\left[\omega\theta^{(s)}(0) + \delta\right] + h$ is fitted at different q values. The best fitting parameters are shown in Tables 3 and 3 for rotating Hayward and Bardeen regular black holes, respectively. The $q = 0$ corresponds to the Kerr black hole. These tables show that only the parameters α and h depend on q. The functions $\alpha(q)$ and $h(q)$ are presented on Fig. 12. These functions are very different for rotating Hayward and Bardeen black holes. The parameters of the fitted quartic polynomials $aq^4 + bq^3 + cq^2 + d$ are listed in Table 3.

Table 3

The coefficients a, b, c and d characterizing the functions $\alpha(q)$ and $h(q)$ for rotating Hayward and Bardeen black holes

$aq^4+bq^3+cq^2+d$	a	b	c	d
$\alpha(q)$ for Hayward	-11.332	5.697	-0.101	-0.111
$\alpha(q)$ for Bardeen	-80.901	-27.243	7.899	-0.111
$h(q)$ for Hayward	65.935	-44.368	0.651	4.554
$h(q)$ for Bardeen	874.359	120.081	-70.979	4.554

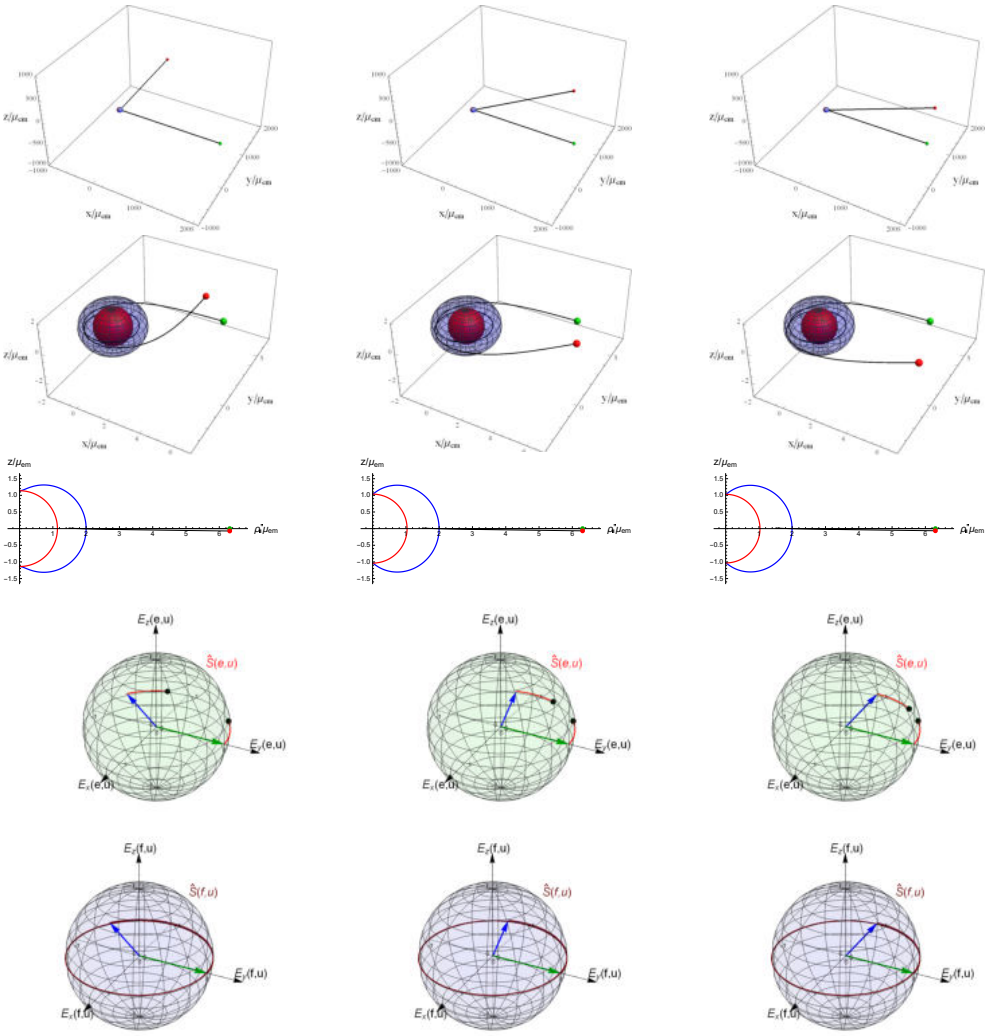

Fig. 1 – The evolutions along unbound orbits. The parameter pair (ν,q) characterizing the central regular black hole changes from left to right as (3,0.081), (3,0.216) and (2,0.081). The rows represent the following: 1st the orbit in the coordinate space (x,y,z), 2nd and 3rd a part of the orbit near the ergosphere in the coordinate spaces (x,y,z) and (ρ,z), respectively, 4th and 5th the unit spin vector in the boosted SO and ZAMO co-moving Cartesian-like frames, respectively. The outer event horizon and the outer stationary surface on the first three rows are depicted by red and blue colors, respectively.

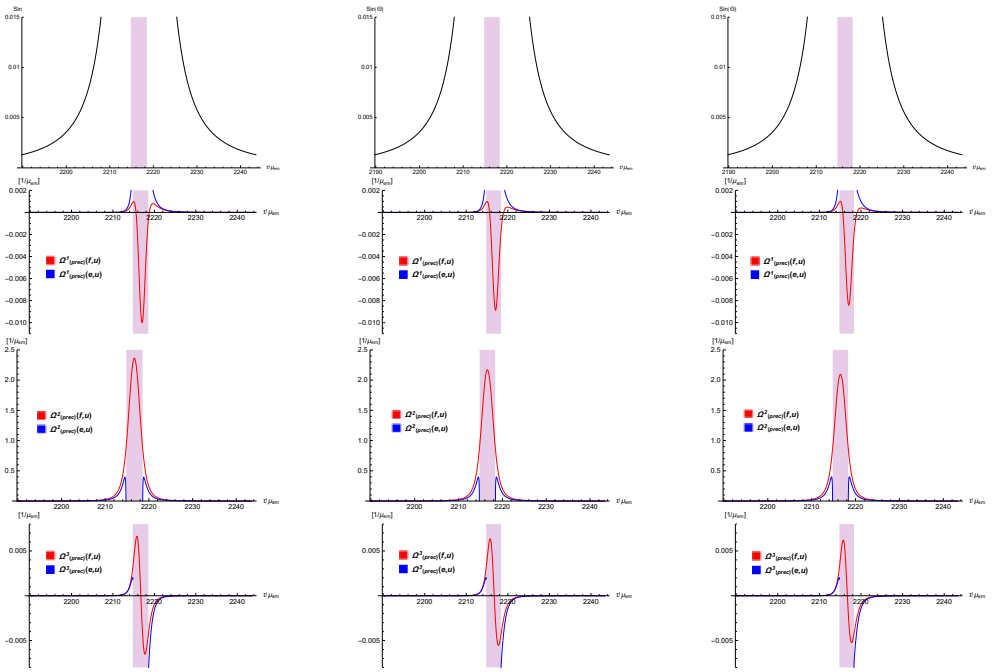

Fig. 2 – The evolution of $\sin\Theta$ and the spherical co-moving triad components of the spin precessional velocities $\Omega^{\alpha}_{(prec)}(e,u)$ and $\Omega^{\alpha}_{(prec)}(f,u)$. The period when the body stays inside the ergosphere is indicated by the purplish shadow.

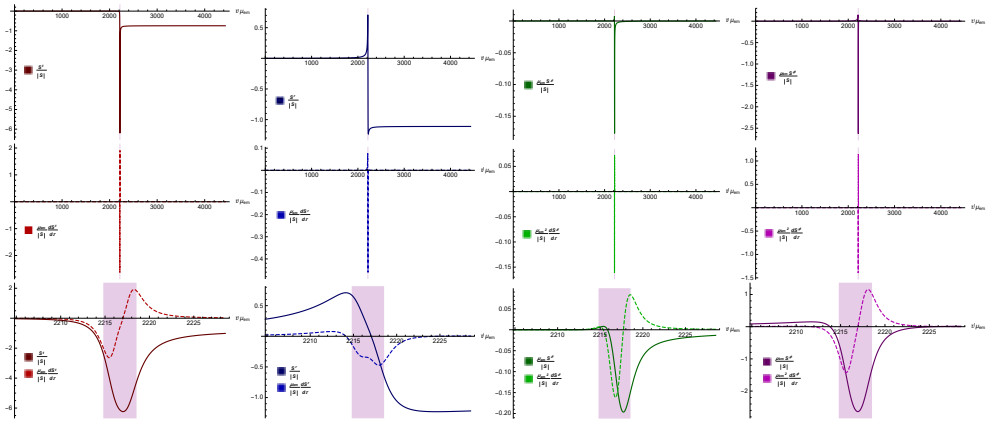

Fig. 3 – The evolution of the Boyer-Lindquist coordinate components of the unit spin vector and their derivatives rescaled to dimensionless variables are presented for the case shown on the middle column of Figs. 1 and 2. The first and the second rows represent the full evolution while the third row zooms in on that period where the body is near and inside the ergosphere, the latter is indicated by the purplish shadow.

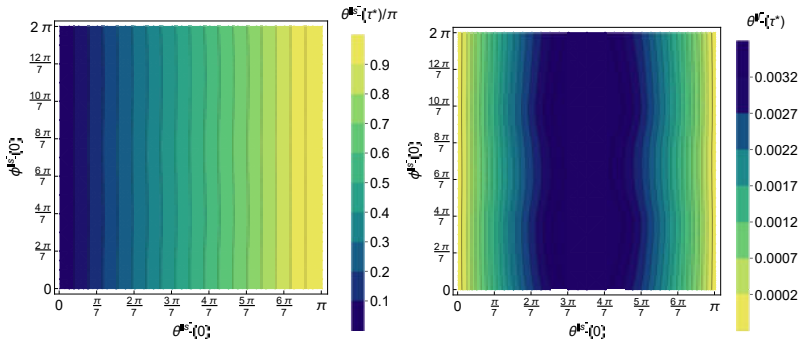

Fig. 4 – The angles $\theta^{(s)}(\tau^*)$ and $\theta^{(l)}(\tau^*)$ as functions of the initial values $\theta^{(s)}(0)$ and $\phi^{(s)}(0)$.

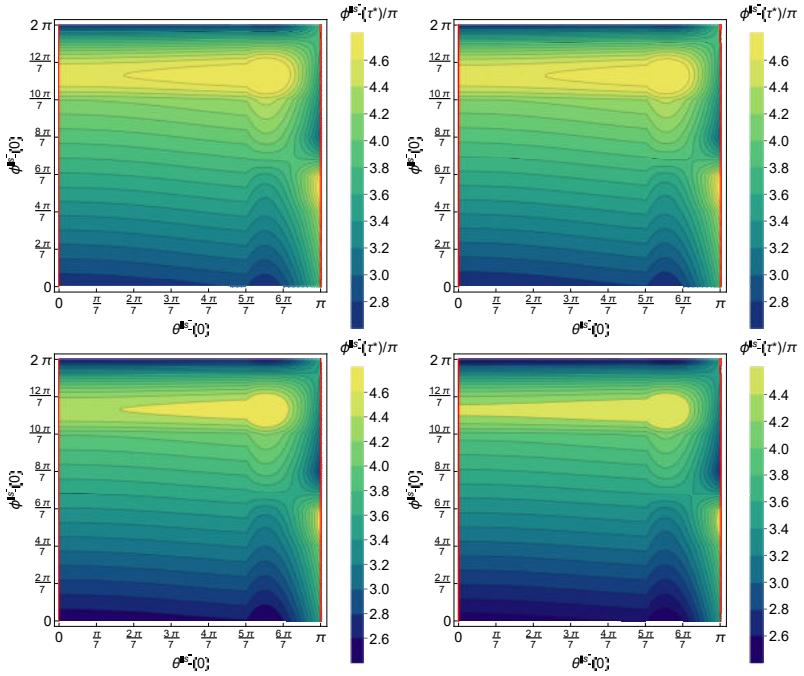

Fig. 5 – The angle $\phi^{(s)}(\tau^*)$ in the parameter space $(\theta^{(s)}(0), \phi^{(s)}(0))$ is shown. From top left to bottom right the background spacetimes are the Kerr, rotating Hayward with $q = 0.081$, rotating Hayward with $q = 0.216$ and rotating Bardeen with $q = 0.081$. The red lines on both sides represent the cases when the azimuthal angle is indefinite.

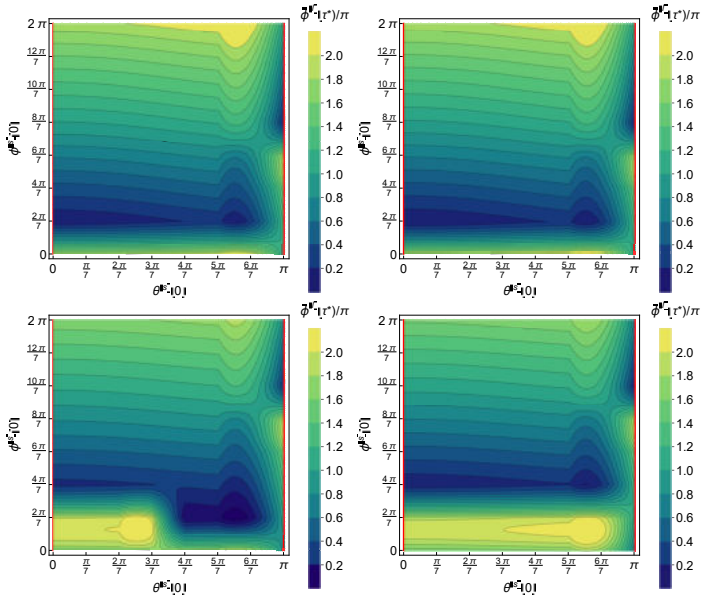

Fig. 6 – The angle $\tilde{\phi}^{(l)}(\tau^*)$ in the parameter space of initial angles $\theta^{(s)}(0)$ and $\phi^{(s)}(0)$. The background spacetime is variated from top left to bottom right such as on Fig. 5. The red lines indicate where $\phi^{(s)}$ is undefined.

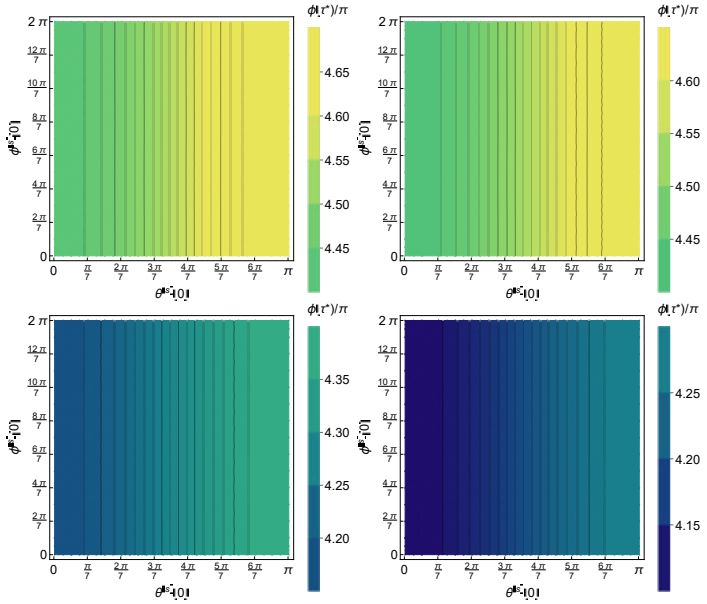

Fig. 7 – The Boyer-Lindquist coordinate $\phi(\tau^*)$ is presented. The background spacetime is variated from top left to bottom right such as on Fig. 5.

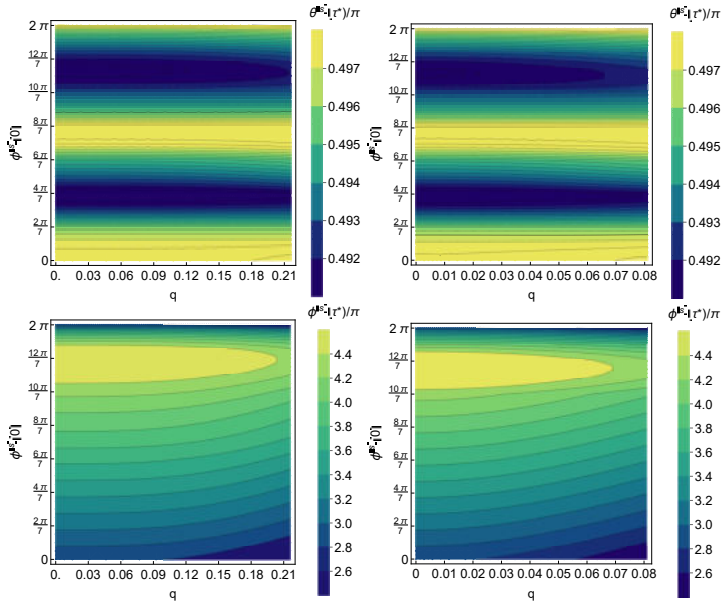

Fig. 8 – The spin angles $\theta^{(s)}(\tau^*)$ and $\phi^{(s)}(\tau^*)$ are shown in the parameter space $(q, \phi^{(s)}(0))$ for rotating Hayward (left col.) and rotating Bardeen (right col.) black holes.

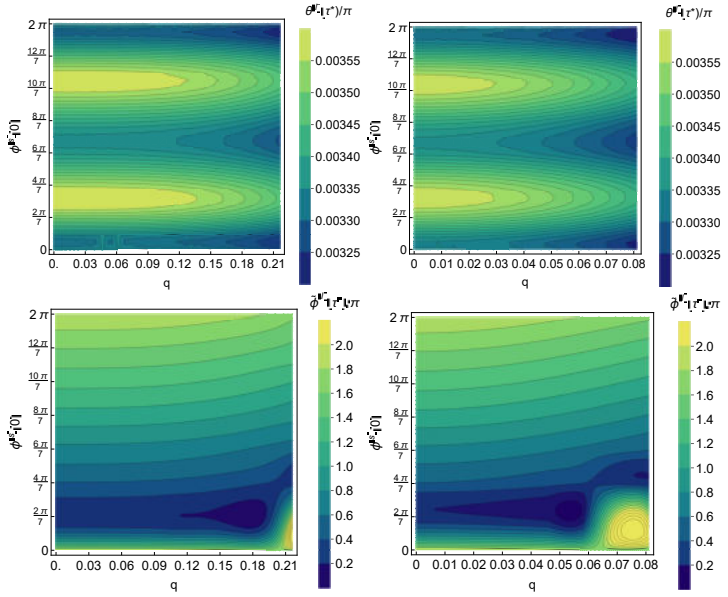

Fig. 9 – The orbital plane orientation angles $\theta^{(l)}(\tau^*)$ and $\tilde{\phi}^{(l)}(\tau^*)$ are shown in the parameter space $(q, \phi^{(s)}(0))$ for rotating Hayward (left col.) and Bardeen (right col.) black holes.

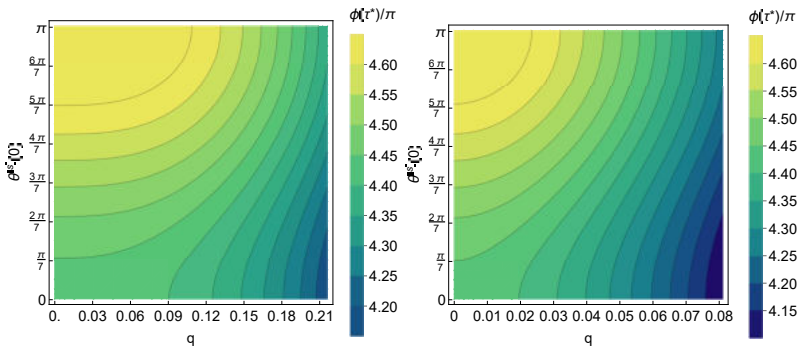

Fig. 10 – The Boyer-Lindquist coordinate $\phi(\tau^*)$ is shown in the parameter space $(q, \theta^{(s)}(0))$ for rotating Hayward (left column) and rotating Bardeen (right column) black holes.

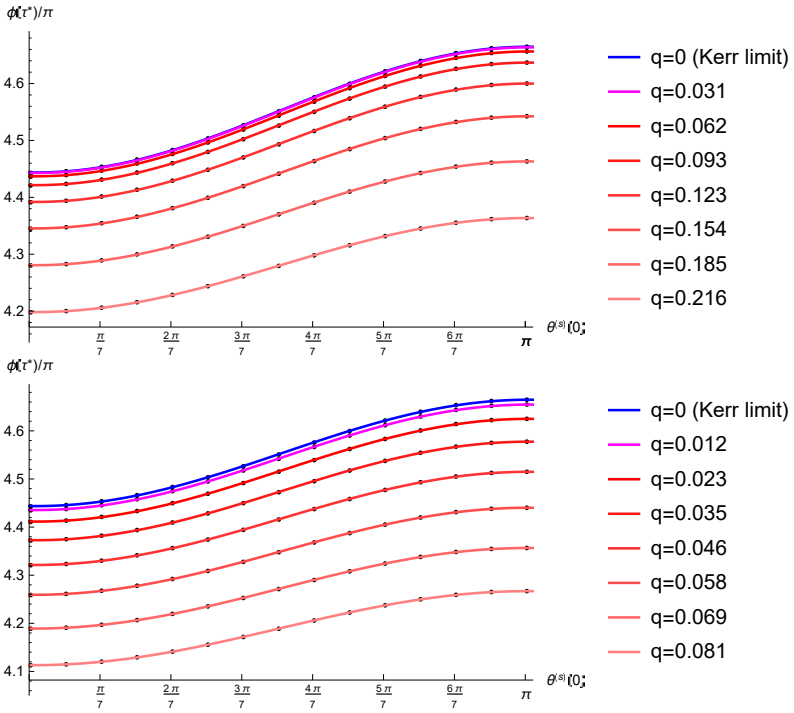

Fig. 11 – The Boyer-Lindquist coordinate $\phi(\tau^*)$ is shown for different q for rotating Hayward (top panel) ($q < 0.216$) and rotating Bardeen (bottom panel) ($q < 0.081$) black holes. The fitted curves are shifted sine functions parametrized as $\alpha \sin(\omega\theta^{(s)}(0) + \delta) + h$. Only the coefficients α and h are q-depend, see Tables 3 and 3.

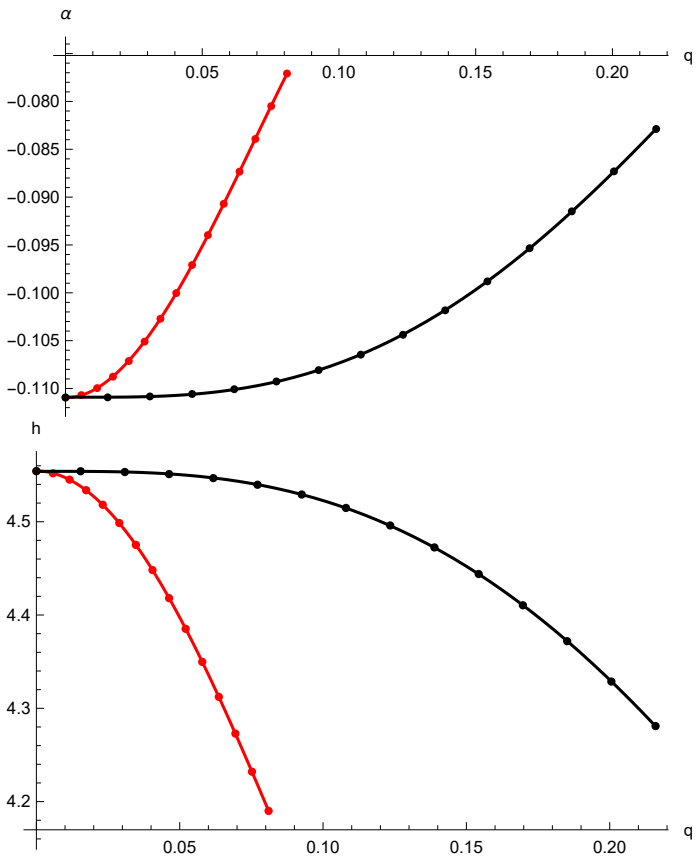

Fig. 12 – The functions $\alpha(q)$ and $h(q)$ for rotating Hayward ($q < 0.216$, black curve) and rotating Bardeen ($q < 0.081$, red curve) black holes.

4. CONCLUSION

We have studied the evolution of spinning bodies moving along unbound orbit in different rotating black hole spacetimes. At the closest approach to the center, the body crossed the ergosphere but remained outside of the outer event horizon. In the considered numerical examples the initial values were chosen such that the relatively small mass body would move in the equatorial plane if it would have no spin or its spin axis would be aligned/anti-aligned with the rotation axis of the central black hole. For other spin configuration the body moved out of the equatorial plane. We have presented that the spin precession was highly increased in the near region of the central black hole especially within the ergosphere.

The numeric investigation indicated that the azimuthal angles $\phi^{(l)}(\tau^*)$, $\phi^{(S)}(\tau^*)$ and $\phi(\tau^*)$ are sensitive for the choice of the parameters ν and q characterizing the regular black hole, while the polar scattering angles $\theta^{(l)}(\tau^*)$ and $\theta^{(S)}(\tau^*)$ are almost insensitive for them. The final value of the Boyer-Lindquist coordinate $\phi(\tau^*)$ is independent from $\phi^{(S)}(0)$ but it is sensitive for $\theta^{(S)}(0)$ and q. The dependence of $\phi(\tau^*)$ on $\theta^{(S)}(0)$ at fixed q value is described by a shifted sine function. Only the amplitude α and the shift parameter h which are q-dependent. The functions $\alpha(q)$ and $h(q)$ are quartic with vanishing linear term. These quartic functions with four parameters together with the frequency and phase shift of the sine function characterize the color map $\phi(\tau^*)$ in the two dimensional space of $\theta^{(S)}(0)$ and q. Apart from the Kerr limit we have found that $\phi(\tau^*)$ is larger for a rotating Hayward black hole than for a rotating Bardeen one for the same q, see Figs. 11 and 12. In addition the derivative $\partial\phi(\tau^*)/\partial\theta^{(S)}(0)$ is also larger in case of a rotating Hayward black hole.

Acknowledgements.
We would like to thank the organizing committee of the RECENT DEVELOPMENTS IN ASTRONOMY, ASTROPHYSICS, SPACE AND PLANETARY SCIENCES Conference for the invitation to this very nice meeting and for the financial support. The work of Z. K. was supported by the János Bolyai Research Scholarship of the Hungarian Academy of Sciences, by the UNKP-19-4 New National Excellence Program of the Ministry of Human Capacities and by the Hungarian National Research Development and Innovation Office (NKFI) in the form of the grant 123996. The work of B. M. was supported by the Hungarian National Research Development and Innovation Office (NKFI) in the form of the grant 116892 and by the János Bolyai Research Scholarship of the Hungarian Academy of Sciences.

REFERENCES

Abdujabbarov, A., Amir, M., Ahmedov, B., and Ghosh, S.G.: 2016, Shadow of rotating regular black holes. *Phys. Rev. D* **93**, 104004.

Ayán-Beato, E., and García, A.: 2000, The Bardeen Model as a Nonlinear Magnetic Monopole. *Phys. Lett. B* **493**, 149.

Bardeen, J.M.: 1968, Non-singular general-relativistic gravitational collapse. *Proc. GR5, Tbilisi USSR*, 174.

Bianchi, E., De Lorenzo, T., and Smerlak, M.: 2015, Entanglement entropy production in gravitational collapse: covariant regularization and solvable models. *JHEP* **06**, 180.

Bini, D., Geralico, A., and Vines, J.: 2017, Hyperbolic scattering of spinning particles by a Kerr black hole. *Phys. Rev. D* **96**, 084044.

Bini, D., Geralico, A., and Jantzen, R.T.: 2017, Gyroscope precession along general timelike geodesics in a Kerr black hole spacetime. *Phys. Rev. D* **95**, 124022.

Bronnikov, K.A.: 2017, Comment on "Construction of regular black holes in general relativity". *Phys. Rev. D* **96**, 128501.

Buchdahl, H.A.: 1972, Characteristic function of Robertson Walker spaces. *Gen. Rel. Grav.* **3**, 35.

Buchdahl, H.A., and N. P. Warner, N.P.: 1980, On the world function of the Godel metric. *J. Phys. A* **13**, 509.

Dixon, W. 1964, A covariant multipole formalism for extended test bodies in general relativity. *Nuovo Cim.* **34**, 317.

Dixon, W.G.: 1970, Dynamics of Extended Bodies in General Relativity. I. Momentum and Angular Momentum. *Proc. R. Soc. London A* **314**, 499.

Dixon, W.G.: 1979, Extended Bodies in General Relativity: Their Description and Motion.*Proceedings of the International School of Physics, Course LXVII, ed. by J. Ehlers*.

Tulczyjew, W.M.: 1959, Motion of multipole particles in general relativity theory. *Acta Phys. Polon.* **18**, 393.

Fan, Z.-Y., and Wang, X.: 2016, Construction of Regular Black Holes in General Relativity. *Phys. Rev. D* **94**, 124027.

Gunther, P.: 1965, Ein Beispiel einer nichttrivialen Huygensschen differentialgleichung mit vier unabhängigen Variablen. *Arch. Rat. Mech. Analys.*, **18**, 103.

Hartl, M.D.: 2003, Dynamics of spinning test particles in Kerr spacetime. *Phys. Rev. D* **67**, 024005.

Hayward, S.A.: 2006, Formation and evaporation of non-singular black holes. *Phys. Rev. Lett.* **96**, 031103.

John, R.W.: 1984, On the calculation of the geodetic distance and associated invariantsin relativistic gravitational fields. *Ann. Phys. Leipzig* **41**, 67.

John, R.W.: 1989, *Trans. Inst. Phys. Estonian Acad Sci.* **65**, 58.

Kerr, R.P: 1963, Gravitational Field of a Spinning Mass as an Example of Algebraically Special Metrics. *Phys. Rev. Lett.* **11**, 237.

Maluf, R.V., and Neves, J.C.S.: 2018, Thermodynamics of a class of regular black holes with a generalized uncertainty principle. *Phys. Rev. D* **97**, 104015.

Mathisson, M.: 1937, Neue Mechanik Materieller Systeme. *Acta. Phys. Polon.* **6**, 163.

Papapetrou, A.: 1951, Equations of Motion in General Relativity. *Proc. Phys. Soc.* **64**, 57.

Roberts, M.D.: 1993, The World Function in Robertson Walker Spacetime. *Astrophys. Lett. Comm.* **28**, 349.

Rodrigues, M.E., and Junior, E.L.B.: 2017, Comment on "Generic rotating regular black holes in general relativity coupled to non-linear electrodynamics". *Phys. Rev. D* **96**, 128502.

Ruse, H.S.: 1960, The potential of an electron in a spacetime of constant curvature. *Quart. J. Math.* **1**, 146.

Semerák, O., 1999, Spinning test particles in a Kerr field - I. *Mon. Not. Roy. Astron. Soc.* **308**, 863.

Synge, J.L.: 1960, Relativity of the general theory. *North-Holland Publishing Company, Amsterdam*.

Toshmatov, B., Abdujabbarov, A., Stuchlík Z., and Ahmedov, B.: 2015, Quasinormal modes of test fields around regular black holes. *Phys. Rev. D* **91**, 083008.

Toshmatov, B., Stuchlík Z., and Ahmedov, B.: 2017, Generic rotating black holes in general relativity coupled to nonlinear electrodynamics. *Phys. Rev. D* **95**, 084037.

Toshmatov, B., Stuchlík, Z., and Ahmedov, B.: 2017, Note on the character of the generic rotating charged regular black holes in general relativity coupled to nonlinear electrodynamics. [arXiv:1712.04763].

Toshmatov, B., Stuchlík, Z., and Ahmedov, B.: 2018, Comment on "Construction of regular black holes in general relativity. *Phys. Rev. D* **98**, 028501.

Toshmatov, B., Stuchlík, Z., Ahmedov, B., and Malafarina, D.: 2019, Relaxations of perturbations of spacetimes in general relativity coupled to nonlinear electrodynamics. *Phys. Rev. D* **99**, 064043.

Vittori, L.D., Gopakumar, A., Gupta, A., Jetzer, P.: 2014, Gravitational waves from spinning compact binaries in hyperbolic orbits. *Phys. Rev. D* **90**, 124066.

Received on 25 November 2019